

# Total Cross Section, Inelasticity and Multiplicity Distributions in Proton – Proton Collisions.

G. Musulmanbekov

Multiparticle production in high energy proton – proton collisions has been analysed in the frame of Strongly Correlated Quark Model (SCQM) of the hadron structure elaborated by the author. It is shown that inelasticity decreases at high energies and this effect together with the total cross section growth and the increasing with collision energy the masses of intermediate clusters result in the violation of KNO – scaling.

## I. INTRODUCTION

In inelastic hadronic interactions with multiparticle production only the fraction of collision energy is converted into the production of secondaries. For the quantitative estimation of this fraction one can use for a given interaction a characteristic, originating from cosmic ray physics, inelasticity, which can be defined as

$$k_1(s) = \frac{M}{\sqrt{s}}, \quad (1)$$

where  $s$  – is square of c.m. energy and  $M$  is the mass of intermediate system which decays into final produced particles. The remaining part of incident energy is carried away by participant's remnants – so-called leading particles. From experimental point of view more suitable is another definition of inelasticity

$$k_2(s) = \frac{1}{\sqrt{s}} \sum_i \int dy \mu_i \frac{dn_i}{dy} \cosh y, \quad (2)$$

where  $\mu_i = \sqrt{p_{Ti}^2 + m_i^2}$  is transverse mass of a produced particle of type  $i$  and  $dn_i/dy$  is its measured rapidity distribution. Fluctuation of inelasticity from event to event leads to the distribution  $P(k)$  with mean inelasticity  $\langle k(s) \rangle$ . The energy dependence of inelasticity is a problem of great interest both from theoretical and experimental points of view. There is no consensus in the physical community on the energy dependence of  $\langle k(s) \rangle$ . The decrease of inelasticity with energy is advocated by some authors [1, 2, 3, 4] while others believe that

inelasticity is an increasing function of energy [5, 6, 7, 8]. The question can not be answered by collider experiments. At ISR energies ( $23 \div 60$  GeV) where leading particle spectrum could be measured the inelasticity defined to be about 0.5. In the collider experiments at higher energies (SPS and Tevatron) leading particles are emitted in an extremely forward cone and could not be measured due to the presence of the beam pipe. Obviously, multiplicity distributions are connected with inelasticity distributions, and so one can study features of multiplicity distributions deriving the information on inelasticity or fraction of the initial energy converted into the particle production. As we know scaled multiplicity distributions exhibit KNO [9] scaling up to ISR energies which is violated for higher energy data (SPS) where they can be described approximately by the negative binomial distribution (NBD). And again at the most high SPS energy, 900 GeV, there is an evident deviation of multiplicity distributions from NBD. In this paper we demonstrate that there is a connection between the energetic behaviour of the shapes of scaled multiplicity distributions and inelasticity distributions which, in turn, relates to the effect of the total cross section growth. For this purpose we use geometrical considerations which are justified by the following arguments. First, hadrons are extended objects with the size about 1 fm and ,second, at high energies de-Broglie wave-length becomes small.

Our analysis is based on the model of hadron structure so-called Strongly Correlated Quark Model (SCQM) [10] which is described in Section 2. In Section 3 the model is applied for the calculation of proton – proton total cross sections and simulation of inelastic events.

## II. STRONGLY CORRELATED QUARK MODEL

The ingredients of the model are the following. A single quark  $q$  of definite colour embedded in vacuum starts to polarize its surrounding that results in the formation of quark and gluon condensate. At the same time it experiences the pressure of vacuum because of zero point radiation field or vacuum fluctuations which act the quark tending to destroy the ordering of the condensate. Suppose that we place the corresponding antiquark in the vicinity of the first one. Owing to their opposite signs colour polarization fields of quark and antiquark interfere destructively in the overlapped space regions eliminating each other at most in the middle-point between the quarks. This effect leads to the decreasing of

condensates density in the same space region and overbalancing of the vacuum pressure acting on quark and antiquark from outer space regions. As a result the attractive force between quark and antiquark emerges and quark and antiquark start to move towards each other. The density of the remaining condensate around quark (antiquark) is identified with the hadronic matter distribution. At maximum displacement in  $\bar{q}q$ - system that corresponds to small overlapping of polarization fields the hadronic matter distributions have maximum extent and magnitude. The closer they to each other, the larger is the effect of mutual destruction and the smaller hadronic matter distributions are around quarks and the larger their kinetic energies. In that way quark and antiquark start to oscillate around their middle-point. For such interacting  $\bar{q}q$ - pair located on  $X$  axis at the distance of  $2x$  from each other the total Hamiltonian is

$$H = \frac{m_{\bar{q}}}{(1 - \beta^2)^{1/2}} + \frac{m_q}{(1 - \beta^2)^{1/2}} + V_{\bar{q}q}(2x), \quad (3)$$

were  $m_{\bar{q}}$ ,  $m_q$  – current masses of valence antiquark and quark,  $\beta = \beta(x)$  – their velocity depending on displacement  $x$  and  $V_{\bar{q}q}$  – quark–antiquark potential energy at separation  $2x$ . It can be rewritten as

$$H = \left[ \frac{m_{\bar{q}}}{(1 - \beta^2)^{1/2}} + U(x) \right] + \left[ \frac{m_q}{(1 - \beta^2)^{1/2}} + U(x) \right] = H_{\bar{q}} + H_q, \quad (4)$$

were  $U(x) = \frac{1}{2}V_{\bar{q}q}(2x)$  is potential energy of quark or antiquark. Quark (antiquark) with the surrounding cloud (condensate) of quark - antiquark pairs and gluons, or hadronic matter distribution, forms the constituent quark. It is natural to assume that the potential energy of quark (antiquark),  $U(x)$ , corresponds to the mass  $M_Q$  of the constituent quark:

$$2U(x) = C_1 \int_{-\infty}^{\infty} dz' \int_{-\infty}^{\infty} dy' \int_{-\infty}^{\infty} dx' \rho(x, \mathbf{r}') \approx 2M_Q(x) \quad (5)$$

where  $C_1$  is a dimensional constant and hadronic matter density distribution,  $\rho(x, \mathbf{r}')$ , is defined as

$$\rho(x, \mathbf{r}') = C_2 |\varphi(x, \mathbf{r}')| = C_2 |\varphi_Q(x' + x, y', z') - \varphi_{\bar{Q}}(x' - x, y', z')|. \quad (6)$$

Here  $C_2$  is a constant,  $\varphi_Q$  and  $\varphi_{\bar{Q}}$  are density profiles of the condensates around quark and antiquark located at distance  $2x$  from each other. Here, we consider that the condensates around quark and antiquark have opposite colour charges. They look like compressive stress and tensile stress (around defects) in solids. The generalization to a three-quark system

in baryons is performed according to  $SU(3)_{\text{color}}$  symmetry: in general, pair of quarks have coupled representations

$$3 \otimes 3 = 6 \oplus \bar{3} \quad (7)$$

in  $SU(3)_{\text{color}}$  and for quarks within the same baryon only the  $\bar{3}$  (antisymmetric) representation occurs. Hence, the antiquark can be replaced by two correspondingly coloured quarks to get a colour singlet baryon and the destructive interference takes place between colour fields of three valence quarks (VQs). Putting aside the mass and charge differences and spins of valence quarks we may say that inside the baryon three quarks oscillate along the bisectors of the equilateral triangle. Therefore, keeping in mind that quark and antiquark in mesons and three quarks in baryons are strongly correlated, we can consider each of them separately as undergoing oscillatory motion under the potential (5) in 1+1 dimension. Hereinafter, we consider VQ oscillating along  $X$ – axis, and  $Z$ – axis is a perpendicular to the plane of oscillation  $XY$ . Density profiles of condensates around VQs are taken in the gaussian form. It has been shown in papers [11] that the wave packet solutions of time dependent Schrodinger equation for a harmonic oscillator move in exactly the same way as corresponding classical oscillators. These solutions are called “coherent states”. This relationship justifies our semiclassical treatment of quark dynamics.

We specify the mass of constituent quark at maximum displacement as

$$M_{Q(\bar{Q})}(x_{\text{max}}) = \frac{1}{3} \left( \frac{m_{\Delta} + m_N}{2} \right) \approx 360 \text{ MeV},$$

where  $m_{\Delta}$  and  $m_N$  are masses delta–isobar and nucleon respectively. The parameters of the model, namely, maximum displacement,  $x_{\text{max}}$ , and parameters of the gaussian function,  $\sigma_{x,y,z}$ , for hadronic matter distribution around VQ are chosen inside the following corridors:

$$x_{\text{max}} = 0.64 \div 0.66 \text{ fm}, \quad \sigma_{x,y} = 0.24 \div 0.28 \text{ fm}, \quad \sigma_z = 0.12 \div 0.20 \text{ fm}. \quad (8)$$

They are estimated by comparison of calculated and experimental values of inelastic cross sections,  $\sigma_{\text{in}}(s)$ , and the inelastic overlap function  $G_{\text{in}}(s, b)$  for  $pp$ – and  $\bar{p}p$ – collisions (see the next section). The current mass of the valence quark is taken to be 5 MeV. The behaviour of potential (5) evidently demonstrates the relationship between constituent and current quark states inside a hadron (Fig. 1). At maximum displacement quark is nonrelativistic, constituent one (VQ surrounded by the condensate), since the influence of polarization fields of other quarks becomes minimal and the VQ possesses the maximal potential energy

corresponding to the mass of the constituent quark. At the origin of oscillation,  $x = 0$ , antiquark and quark in mesons and three quarks in baryons, being close to each other, have maximum kinetic energy and correspondingly minimum potential energy and mass: they are relativistic, current quarks (bare VQs). This configuration corresponds to so-called “asymptotic freedom” . In the intermediate region there is increasing (decreasing) of the constituent quark mass by dressing (undressing) of VQs due to decreasing (increasing) of the destructive interference effect. The evolution of colour charge density profiles of quark – antiquark pair during the half-period of oscillation is shown in Fig. 2. Here, we suppose that the quark colour charge is positive and the antiquark color charge is negative.

The proposed dynamical picture meets local gauge invariance principle. Indeed, destructive interference of color fields of quark and antiquark in mesons and three quarks in baryons depending on their displacements can be treated as a phase rotation of wave function of a single VQ in colour space  $\psi_c$  on angle  $\theta$  depending on the displacement  $x$  of the VQ in the coordinate space

$$\psi_c(x) \rightarrow e^{ig\theta(x)}\psi_c(x). \quad (9)$$

The color phase rotation, in turn, leads to VQ dressing (undressing) by quark and gluon condensate that corresponds to the transformation of a gauge field

$$A_\mu(x) \rightarrow A_\mu(x) + \partial_\mu\theta(x). \quad (10)$$

Here, we drop colour indices of  $A_\mu(x)$  and consider each quark of specific colour separately as changing its effective colour charge,  $g\theta(x)$ , in color fields of other quarks (antiquark) due to the destructive interference. Thus, gauge transformations (9), (10) map internal (isotopic) space of a colored quark onto the coordinate space. On the other hand, this dynamical picture of VQ dressing (undressing) corresponds to the chiral symmetry breaking (restoration). Due to this mechanism of VQs oscillations the nucleon runs over the states corresponding to the certain terms of the infinite series of Fock space

$$|B\rangle = c_1 |q_1 q_2 q_3\rangle + c_2 |q_1 q_2 q_3 \bar{q} q\rangle + c_3 |q_1 q_2 q_3 g\rangle \dots \quad (11)$$

The proposed model has some important consequences. Inside hadrons the valence quarks and accompanying them gluons and quark-antiquark pairs, as well, are strongly correlated. Nucleons are nonspherical object: they are flattened along the axis perpendicular to the plane of quarks oscillations.

From the form of the quark potential (Fig. 1) one can conclude that dynamics of VQ corresponds to nonlinear oscillator and VQ with its surrounding can be treated as a nonlinear wave packet. Moreover, our quark – antiquark system turned out to be identical to so-called “breather” solution of (nonlinear) sine–Gordon (SG) equation[12]. SG equation in (1+1) dimension in the reduced form for scalar function  $\phi(x, t)$  is given by

$$\square\phi(x, t) + \sin\phi(x, t) = 0, \quad (12)$$

where  $x, t$ -dimensionless. Breather is a periodic solution representing a bound state of a soliton-antisoliton pair which oscillates around its center of mass:

$$\phi_{br}(x, t) = 4 \tan^{-1} \left[ \frac{\sinh \left[ ut / \sqrt{1 - u^2} \right]}{u \cosh \left[ x / \sqrt{1 - u^2} \right]} \right], \quad (13)$$

where  $u$  is 4-velocity. During the oscillations of the soliton-antisoliton pair their density profile

$$\varphi_{br}(x, t) = \frac{d\phi_{br}(x, t)}{dx} \quad (14)$$

evolves like our quark–antiquark system, i.e. at the maximal displacement the soliton and antisoliton are emphasized maximal and at the minimum displacement they “annihilate” (Fig. 3). This similarity is not surprising because our quark–antiquark system was formulated in close analogy with the model of dislocation-antidislocation which in the continuous limit is described by the breather solution of SG equation [13]. It can be shown that soliton, antisoliton and breather obey relativistic kinematics, i.e. their energies, momenta and shapes are transformed according to Lorentz transformations. Since the above consideration of quarks as solitons is purely classical the important problem is to construct quantum states around them. Although the soliton solution of SG equation looks like an extended (quantum) particle the relation of classical solitons to quantum particles is not so trivial. The technique of quantization of the classical solitons with the usage of various methods has been developed by many authors. The most known of them is semiclassical method of quantization (WKB) which allows one to relate classical periodic orbits (breather solution of SG) with the quantum energy levels [14].

Hereinafter, we adhere to our semiclassical model (SCQM) applying it for analysis of cross sections and the multiparticle production in hadron–hadron collisions.

### III. HADRON - HADRON COLLISIONS

Different configurations of the quark content inside a hadron realized at the instant of the collision result in different types of reactions. The probability of finding any quark configuration inside the hadron is defined by the probability of VQ's displacement in a proper frame of the hadron:

$$P(x)dx = \frac{Adx}{\sqrt{1 - m_q^2/[E_q - U(x)]^2}}, \quad (15)$$

where  $E_q$  is a total energy of the valence quark (antiquark) and a constant  $A$  can be derived from the normalization condition

$$\int_{-\infty}^{\infty} P(x)dx = 1. \quad (16)$$

Configurations with nonrelativistic constituent quarks ( $x \simeq x_{\max}$ ) in both colliding hadrons lead to soft interactions with the nondiffractive multiparticle production in central and fragmentation regions (Fig. 4a). The hard scattering with the jet production and the large angle elastic scattering take place when configurations with current VQs ( $x \simeq 0$ ) in both colliding hadrons are realized (Fig. 4b). The near current quark configuration inside one of the hadrons and constituent quark configuration inside the second one result in single diffraction scattering (Fig. 4c). And at last intermediate configurations inside one or both hadrons are responsible for semihard and double diffractive scattering (Fig. 4d). The same geometrical consideration can be applied to deep inelastic scattering processes if one assumes that a real or virtual photon converts into the vector meson according to the vector dominance model.

First, we apply our model for the calculation of proton-proton and antiproton-proton cross sections at high energies and demonstrate that the growth of the cross section with energy is caused by predominantly increasing contribution of peripheral interactions that, in turn, leads to the decreasing of inelasticity of collisions. Then we will show that the energetic behaviour of inelasticity distributions governs the energetic behaviour of scaled multiplicity distributions.

### A. Cross Sections

To calculate cross sections we used an impact parameter representation, namely Inelastic Overlap Function (IOF), which can be specified via the unitarity equation

$$2\text{Im}f(s, b) = |f(s, b)|^2 + G_{\text{in}}(s, b), \quad (17)$$

where  $f(s, b)$ —elastic scattering amplitude and  $G_{\text{in}}(s, b)$  is IOF. IOF is connected with inelastic differential cross sections in impact parameter space:

$$\frac{1}{\pi}(d\sigma_{\text{in}}/db^2) = G_{\text{in}}(s, b). \quad (18)$$

Then the inelastic, elastic and total cross sections can be expressed via IOF as

$$\sigma_{\text{in}}(s) = \int G_{\text{in}}(s, \mathbf{b}) d^2\mathbf{b}, \quad (19)$$

$$\sigma_{\text{el}}(s) = \int \left[1 - \sqrt{1 - G_{\text{in}}(s, \mathbf{b})}\right]^2 d^2\mathbf{b}, \quad (20)$$

$$\sigma_{\text{tot}}(s) = 2 \int \left[1 - \sqrt{1 - G_{\text{in}}(s, \mathbf{b})}\right] d^2\mathbf{b}. \quad (21)$$

Since IOF relates to the probability of inelastic interaction at a given impact parameter, we carried out Monte Carlo simulation of inelastic nucleon–nucleon interactions. The Inelastic interaction takes place at the definite impact parameter  $b$  if the produced mass meets the following requirement:

$$M_{CF}^2 = 4M_P\gamma_P M_T\gamma_T \int \rho_P(\mathbf{r})\rho_T(\mathbf{r} - \mathbf{b}) d^3\mathbf{r} \geq (M_{CF}^2)_{\text{min}}, \quad (22)$$

where  $M_{CF}$  is the mass of the central “fireball” produced at the overlapped region,  $\rho_P$  and  $\rho_T$  are hadronic matter density distributions in projectile and target hadrons,  $M_P$ ,  $M_T$  – masses,  $\gamma_P$ ,  $\gamma_T$  – gamma-factors of the colliding hadrons and  $(M_{CF}^2)_{\text{min}}$  – the minimal mass of a fireball that results in an inelastic event. This expression is the modification of assumption of Heisenberg [15] on interaction of extended particles: we replaced in his original formula the pion mass squared (on the right hand side) by  $(M_{CF}^2)_{\text{min}}$ . In our previous papers this quantity corresponded to the transverse mass of the pion:  $m_{\pi\perp}^2 = p_{\perp}^2 + m_{\pi}^2$ . Taking into account the energy dependence of the average momentum of produced particles and the increasing yield of minijets (as treated in what follows) we parametrize the minimal fireball mass as

$$(M_{CF})_{\text{min}} = 0.3 + 0.03s^{1/4}. \quad (23)$$



Specifying the quark configurations in each colliding hadrons according to (15) we calculated  $G_{\text{in}}(s, b)$  for particular values of the impact parameter  $b$  and then according to (21) – total cross sections,  $\sigma_{\text{tot}}$ . Fig. 5 shows the results of the calculation for total cross sections for proton – proton and antiproton – proton collisions in a wide range of collision energies. One can see that the model with fixed parameters characterizing the geometrical size of hadrons describes the energetic behaviour of  $\sigma_{\text{tot}}$  rather well. The growth of the total cross section with energy coming from the growth of the inelastic cross section is due to the continuous tails of condensates (hadronic matter distributions) around VQs not compensated by the destructive interference effect inside each interacting particle. With rising collision energy the overlap of more peripheral parts of these tails make it possible to meet requirement (22) and consequently results in the increasing effective size of the hadronic matter distribution inside nucleons and correspondingly the increasing radius of interactions. It can be seen from the comparison of IOFs for ISR and SPS energies which is given in Fig. 6. According to Eq. (18) the difference  $G_{\text{in}}^{\text{SPS}} - G_{\text{in}}^{\text{ISR}}$  exhibits the predominantly peripheral increase of the inelastic cross section (and thus of the total cross section, since  $\sigma_{\text{el}}/\sigma_{\text{tot}}$  is only about 20%) which is centered around 1 fm (Fig. 6b). As noted by the authors of the paper [17] at high energies colliding nucleons become blacker, edger and larger (“BEL-effect”). The model gives the linear logarithmic energy dependence for total cross sections. At energies  $\sqrt{s} < 30$  GeV calculated cross sections were corrected on contributions of Regge poles exchange by using Donnachie and Landshoff parametrization[18]. An oscillatory motion of VQs appearing as an interplay between constituent and bare (current) quark configurations results in fluctuations of the hadronic matter distribution inside colliding nucleons. The manifestation of these fluctuations is a variety of scattering processes, hard and soft, in particular, the process of single diffraction (SD). SD-events correspond to the constituent quark configuration inside one colliding hadron and (semi)bare quark configuration inside the other one. Our unified geometrical explanation of diffractive, nondiffractive and DIS processes could give an answer to the long standing question: what is pomeron? Historically the concept of “Pomeron” originating from simple Regge pole with the intercept  $a_0 = 1$  transformed to a rather complicated object with relatively arbitrary features and smooth meaning. To produce the rising cross sections it must have the intercept such that  $a_0 = 1 + \varepsilon$ . The fact that the parameter  $\varepsilon$  is universal, independent of particles being scattered in hadronic and DIS interactions, could say us that the nature of the cross section growth is the same for

all processes. Our interpretation of pomeron is a geometrical one. Both diffractive and nondiffractive particle productions emerge from the disturbance (excitation) of overlapped continuous vacuum polarization fields (gluon and  $\bar{q}q$  condensate) around valence quarks of colliding hadrons followed by fragmentation process. The type of the interaction depends on quark configurations inside a colliding hadron occurring at the instant of the interaction and the value of the impact parameter. So, what we used to call “Pomeron” in  $t$ - channel is solely continuum states in  $s$ - channel and we claim that Pomeron is unique in elastic, inelastic (diffractive and nondiffractive) and DIS.

### B. Multiparticle Production in Hadronic Collisions

According to our model the configurations with nonrelativistic constituent quarks ( $x \simeq x_{max}$ ) inside the both colliding hadrons lead to soft interactions with multiparticle production in central and fragmentation regions. The additional restriction by small impact parameters selects central collisions when hadronic matter distributions of colliding hadrons (quarks) overlap totally. In this case kinetic energies of colliding hadrons dissipate totally converting into the production of secondary particles that corresponds to collision inelasticity close to 1 and very high multiplicity in comparison with the mean one. We will consider the soft interactions and nondiffractive multiparticle production, in particular. According to the KNO hypothesis the scaled multiplicity distributions,  $\langle n \rangle P_n(s)$ , depend on the ratio of the number of particles to the average multiplicity  $z = n / \langle n \rangle$  and they are energy independent. From our geometrical point of view such behaviour could be explained as a superposition of relatively narrow distributions corresponding to the particular impact parameters of the collisions. Indeed, the multiplicity distribution can be defined as

$$P_n(s) = \int_0^1 P(n | k) P[k(s)] dk, \quad (24)$$

where  $P[k(s)]$  is inelasticity distribution and  $P(n | k)$  is the probability of the production of  $n$  particles at the given inelasticity,  $k$ . So, if the conditional probability  $P(n | k)$  is sufficiently narrow then the shape of the distribution  $P_n$  is defined by the shape of the inelasticity distribution  $P[k(s)]$ . The inelasticity distributions are strictly connected with the impact parameter distributions. KNO scaling holds (at least, approximately) if the impact parameter distributions and consequently inelasticity distributions are energy independent.

As shown in the previous subsection the growth of inelastic and total cross sections with energy in hadronic collisions is due to the increasing of effective sizes of interacting hadrons. To make a quantitative analysis of energetic dependence of multiplicity distributions we performed, in the frame of SCQM, Monte Carlo simulation of inelastic proton – proton interactions selecting nondiffractive events. The process of simulation includes the following steps.

1. Applying Heisenberg prescription (22) we define the mass of the central “fireball” (CF) (Fig. 7) produced in the proton–proton collision at a particular impact parameter. Quark configurations inside each proton at the instant of the collision is specified randomly according to the probability (15) that allows one to fix energies and momenta of quarks inside both protons. Since the mass of CF is formed by the overlap of hadronic densities of individual constituent quarks (CQ) of colliding protons we know the energies and momenta of quarks in both remnants which we call, by convention, forward and backward “fireballs” (FF and BF). The notion “fireball” is applied by convention only because all fireballs, CF, FF and BF, can decay string – like manner and there is no sharp boundary between secondaries emitted from fireballs in the rapidity space for nondiffractive events. Then we calculate the effective masses of FF and BF (Fig. 7):

$$M_{FF} = \sqrt{\left(\sum_{i=1}^3 E'_i\right)^2 - \left(\sum_{i=1}^3 \mathbf{k}_i\right)^2}, \quad (25)$$

$$M_{BF} = \sqrt{\left(\sum_{i=4}^6 E'_i\right)^2 - \left(\sum_{i=4}^6 \mathbf{k}_i\right)^2}, \quad (26)$$

where  $E'_i$  and  $\mathbf{k}_i$  are energies and momenta of constituent quarks after the collision.

2. We assume that each fireball breaks up, in general, into clusters. Here, the bremsstrahlung analogy is used, namely, at the instant of the collision a proton (electron) loses the energy dumping fraction of its hadronic (electromagnetic) field by means of the emission of clusters (photons). To simulate the masses of the clusters we apply the result of the paper [19] for a cluster mass spectrum

$$P(m_{cl}) = (m_{cl}/m_0) \exp(-m_{cl}/m_0), \quad (27)$$

following from the statistical nature of the cluster emission. Our next assumption is that masses of clusters increase with the collision energy. This is dictated by the necessity to take into account such peculiarities of multiparticle production as the growth of rapidity distribution plateau, the increasing of transverse momenta of secondaries and the increasing yield of minijets. We parametrize the energy dependence of the average mass of clusters as

$$\langle m_{cl} \rangle = 0.3 + 0.09s^{1/4}. \quad (28)$$

Notice that we have chosen the same energetic dependence for the minimal fireball mass in Heisenberg prescription (23) except for the value of the slope parameter.

3. Given the positions of the centers of masses of each fireball in rapidity space and kinematically allowed rapidity (sub)spaces for the breaking up of each fireball into clusters we simulate the momenta for each generated cluster in the proper frame of the corresponding fireball. Bremsstrahlung mechanism of the fireball fragmentation corresponds to statistically independent emission of clusters with the limited transverse momenta. Therefore, we apply the cylindrical phase space model according to which the rapidity of  $i$ -th cluster is defined as

$$y_i = \xi Y_i, \quad (29)$$

where  $\xi$  is random number uniformly distributed in the interval  $[0,1]$ . The allowed rapidity interval,  $Y_i$ , is given by

$$Y_i = \ln(M_F^2/(\mu_{cl})_i^2),$$

where  $(\mu_{cl})_i^2 = (m_{cl})_i^2 + p_{\perp i}^2$ , transverse mass of the cluster  $i$ . Moreover, the rapidity interval for fragmentation of the central fireball,  $Y_i^{CF}$ , is restricted by the requirement

$$Y_i^{CF} \leq Y^{FF} - Y^{BF}, \quad (30)$$

where  $Y^{FF}$  and  $Y^{BF}$  are rapidities of forward and backward fireball respectively. The transverse momenta of the clusters are generated according to the distribution

$$f(p_{\perp}^2) \propto \exp(-bp_{\perp}^2). \quad (31)$$

The energy of the remnant baryon in the proper frame of FF (BF) is defined by the summary energy of two quarks closest to each other in rapidity space, i.e. kinematic characteristics of the baryon are connected to those of “diquark”.

4. Since our clusters are identified with minijets they should decay in a jet-like manner. One could assume that these minijets are formed by the fragmentation of the excited sea quark–antiquark pair. Hence, we can approximate the spectrum of cluster decay using data on the electron–positron annihilation provided that the cluster mass is identified with the center of mass energy of an electron and positron:  $m_{cl} = \sqrt{s_{e^+e^-}}$ . One can apply for this purpose any of appropriate Monte – Carlo generators. The axis of the decaying jet is generated to be directed isotropically. And, at last, the model meets energy – momentum conservation requirements for all products of a reaction.

Calculated in such a manner the multiplicity distributions in the KNO form and the energetic dependence of the mean multiplicity for charged particles are shown in Figures 8 and 9. Given all characteristics of produced particles in the event we can calculate inelasticity  $k_2$  (Eq. 2). Its distributions for  $pp$ – interactions at different collision energies are shown in Fig. 10. The inelasticity distribution evolves with energy in such a way that its maximum position shifts to the lower values of inelasticity at higher collision energies. It means that the higher is the collision energy the lower is the average inelasticity (Fig. 11). Analyzing the multiplicity distribution at different energies one can see that its maximum position shifts to the lower values of scaled multiplicities and the contribution of high multiplicities increases while the collision energy increases. According to Eq. (24) the multiplicity distribution can be expressed via the conditional multiplicity distribution at particular inelasticity and the inelasticity distribution. The conditional multiplicity distribution at the particular inelasticity, in turn, is built from multiplicities of clusters emitted from forward, backward and central fireballs and multiplicities going from the clusters’ fragmentation. If the inelasticity distribution and (average) mass of the clusters would not depend on the collision energy then the scaled multiplicity distributions do not depend on energy either and KNO - scaling takes place. The shift of the position of the maximum of the inelasticity distribution with the energy growth shifts the position of the scaled multiplicity distribution. On the other hand, masses of clusters growing with collision

energy lead to the narrowing of available rapidity space and, consequently, to the violation of Feynman scaling. This effect most obviously exhibiting at the inelasticities close to 1 cause the lift of a multiplicity distribution tail at high multiplicities. To summarize we claim that the mean inelasticity decreases with energy, and the violation of KNO - scaling is a consequence of the growth of inelastic and total cross sections and of masses of emitted clusters with energy.

This research was partly supported by the Russian Foundation of Basics Research, grant 01-07-90144.

- 
- [1] G. Fowler, R. M. Weiner, G. Wilk, Phys. Rev. Lett., **55** (1985) 177.
  - [2] Z. Wlodarczyk, J. Phys. G: Nucl. Part. Phys., **19** (1993) L128.
  - [3] Yu. A. Shabelski *et al.*, J. Phys. G: Nucl. Part. Phys., **18** (1992) 1281.
  - [4] Y. D. He, J. Phys. G: Nucl. Part. Phys., **19** (1993) 1953.
  - [5] J. Dias de Deus, Phys. Rev. D **32** (1985) 334.
  - [6] Gaisser T. K. and Stanev T., Phys. Lett., B219 (1989) 375.
  - [7] Kopeliovich B. Z., Nikolaev N. N. and Potashikova I. K., Phys. Rev. D **39** (1989) 769.
  - [8] F. S. Duraes, F. O. Navarra and G. Wilk, Phys. Rev., D47 (1993) 3049.
  - [9] Z. Koba, N. B. Nielsen and P. Olesen, Nucl. Phys., **B40** (1972) 317
  - [10] G. Musulmanbekov, *Proc. VIIIth Blois Workshop*, Ed. V. A. Petrov, World Scientific, 2000, p. 341–350, and references therein.
  - [11] E. Schrodinger, Naturwissenschaften **14** (1926) 664.
  - [12] G. Musulmanbekov in *Frontiers of Fundamental Physics 4*, Ed. B. G. Sidharth, Kluwer Acad. Press, 2001, p. 109–120.
  - [13] R. Rajaraman, Phys. Rep. **21C** (1975) 229.
  - [14] R. Dashen, B. Hasslacher and a. Neveu, Phys. Rev. **D10** (1974) 4114.
  - [15] W. Heisenberg, Zeit. Phys., Bd. 133 (1952) 65.
  - [16] <http://durpdg.durham.ac.uk/HEPDATA>.
  - [17] R. Henzi and P. Valin, Phys. Lett. **132B** (1983) 443; R. Henzi, Proc. of the 4th Topical Workshop on  $\bar{p}p$  Collider Physics, Bern, 1984.
  - [18] A. Donnachie and P. V. Landshoff, CERN-TH 6635/92.
  - [19] Chou Kuang-chao, Liu Lian-son, Meng Ta-chung, Phys. Rev., **D28** (1983) 1080.
  - [20] V. S. Barashenkov, N. B. Slavin, Acta Phys. Pol., **B12** (1981) 563.

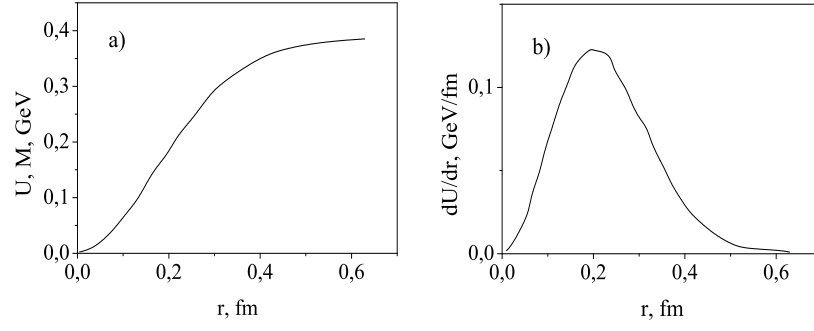


FIG. 1: a) Potential energy of valence quark and mass of constituent quark; b) "Confinement" force.

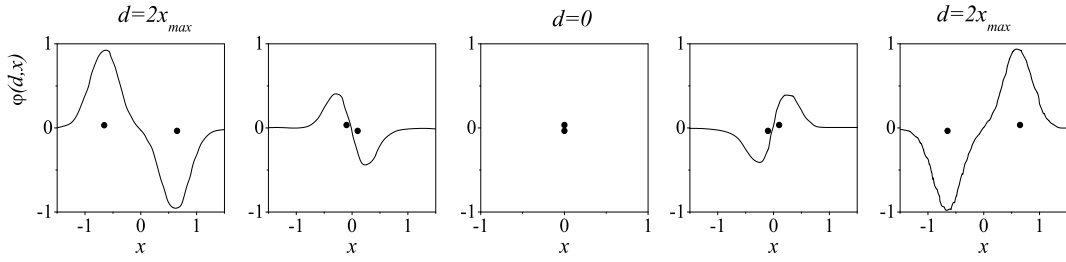


FIG. 2: Evolution of color charge density profile,  $\varphi$ , in quark-antiquark system during half-period of oscillations;  $d = 2x$  – distance in *fermi* between quark and antiquark depicted as dots.



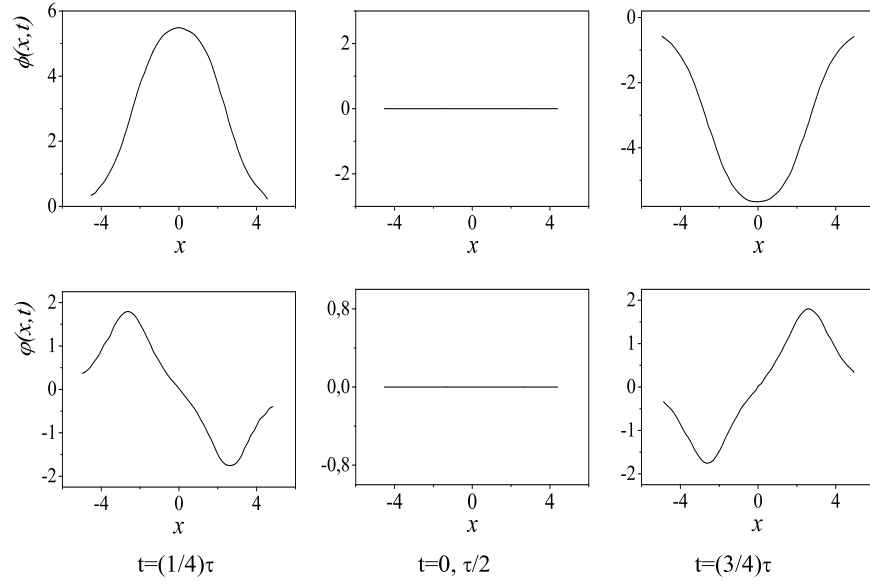


FIG. 3: Evolution of breather,  $\phi$ , and its energy density profile,  $\varphi$ , during a half-period of oscillation. Scales are arbitrary.

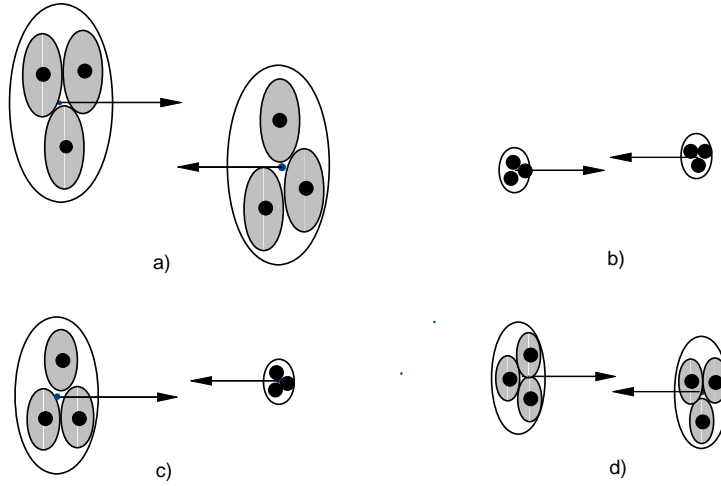


FIG. 4: Different quark configurations realized inside colliding nucleons at the instant of collision.

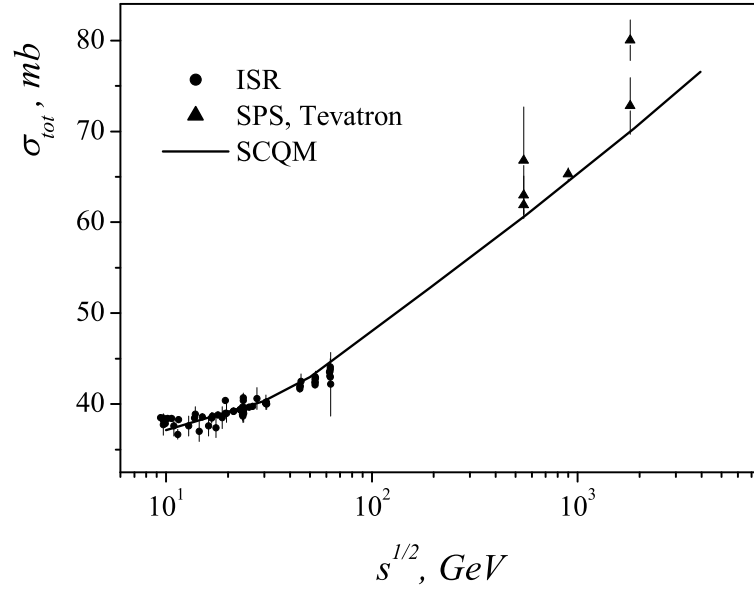


FIG. 5: Total cross section for  $pp$  and  $\bar{p}p$ . Data are taken from electronic data base HEPDATA [16].

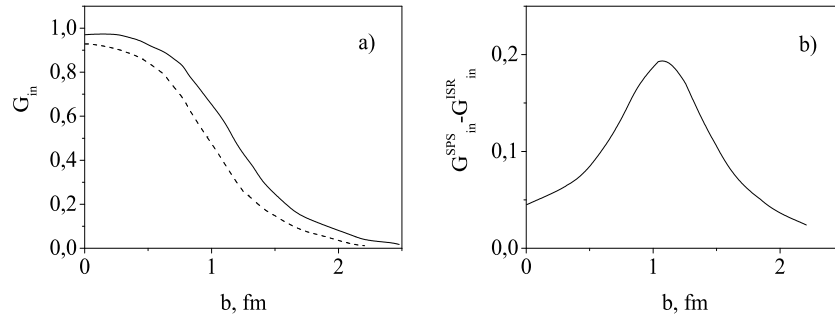


FIG. 6: Plot of overlap functions at ISR and SPS energies, (a), and the difference of overlap functions  $G_{in}^{SPS} - G_{in}^{ISR}$ , (b), as a function of impact parameter  $b$ .

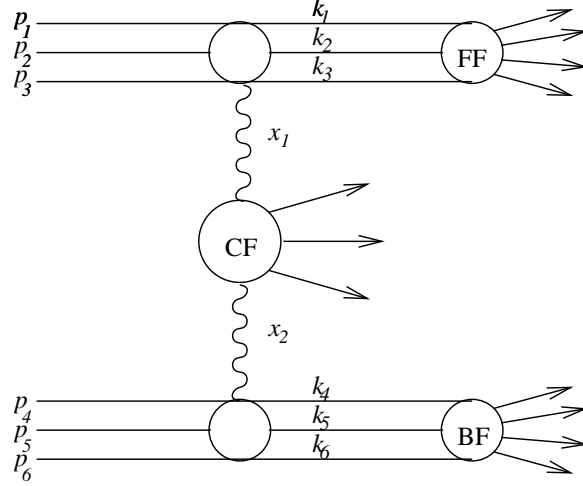


FIG. 7: Fireball picture of multiparticle production in proton – proton collision.  $p_i$  and  $k_i$  are momenta of constituent quarks before and after collision, respectively;  $x_1$  and  $x_2$  – fractions of protons momenta forming the central fireball.

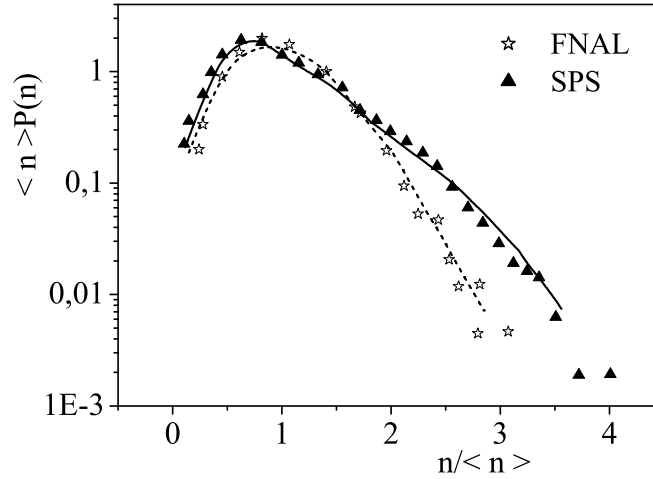


FIG. 8: The multiplicity distributions of charged particles in  $pp$ - and  $\bar{p}p$ - collisions. Data are taken from electronic data base HEPDATA [16].

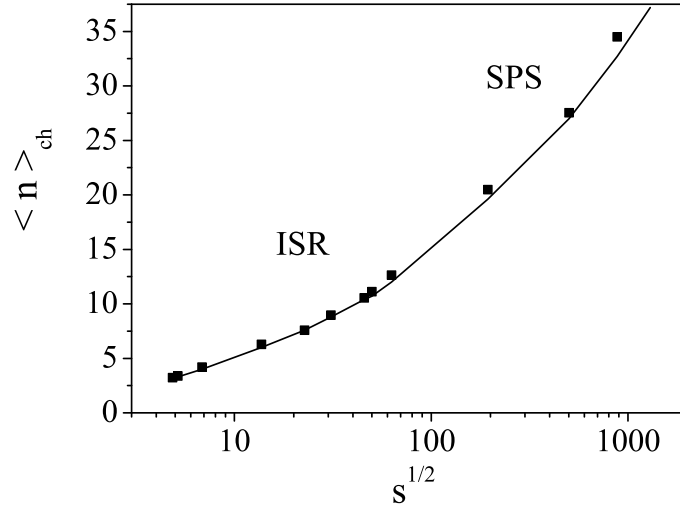


FIG. 9: The energetic dependence of the average multiplicity of charged particles in  $pp$ - and  $\bar{p}p$ - collisions. Data are taken from electronic data base HEPDATA [16].

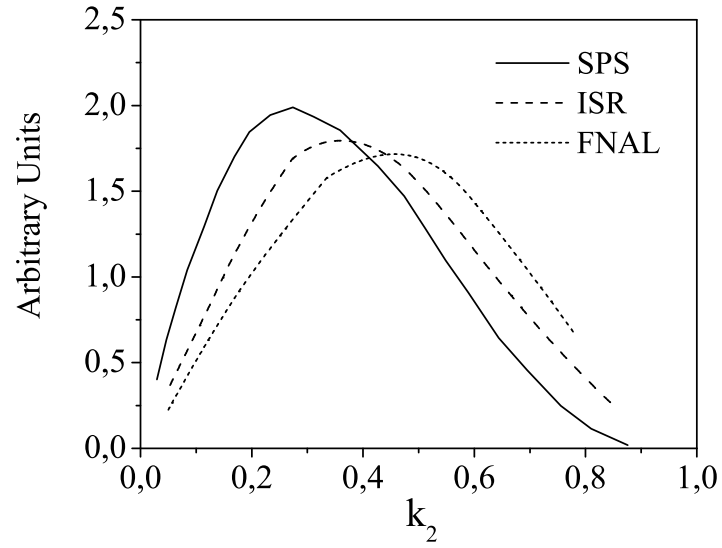


FIG. 10: Inelasticity distributions for  $pp$ - and  $\bar{p}p$ - collisions calculated according to Eq. (2).

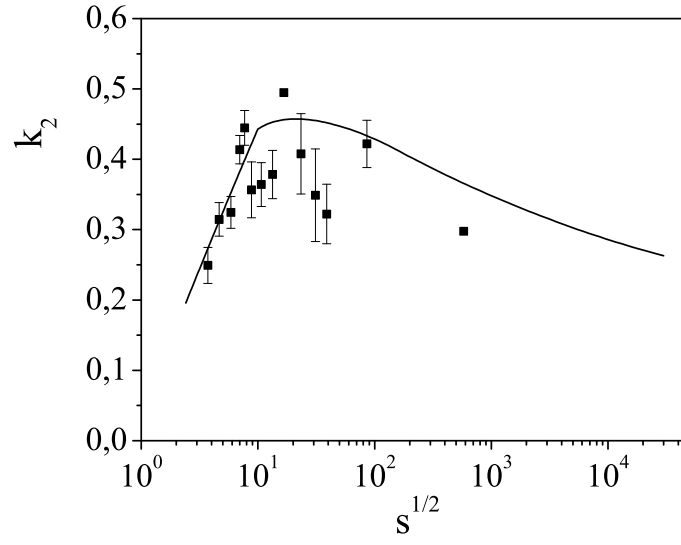


FIG. 11: The average inelasticity plotted as a function of the energy for  $pp$ - and  $\bar{p}p$ - collisions. Boxes are compilation of data given in paper [20].